18th Brazilian Congress of Thermal Sciences and Engineering
November 16-20, 2020 (Online)

ENC-2020-0484
EXERGETIC ANALYSIS OF A HYBRID SOLAR-BIOMASS POWERPLANT

Marcela Alves Domingues
Renan Manozzo Galante
Universidade Tecnológica Federal do Paraná, Department of Mechanical Engineering, Campus Guarapuava, Avenida Professora Laura Pacheco de Bastos, 800, CEP 85053-525, Guarapuava- PR, Brazil.
marceladomingues@alunos.utfpr.edu.br; rmgalante@utfpr.edu.br

Abstract. *The discussion on the use of renewable sources for power generation has increased on the past decades due to its importance on environmental and economic aspects. This work focus on a hybrid solar-biomass energy configuration, applying two renewable energy sources to maintain a constant supply of electricity without the need of thermal or electrical storage. A model for an operating 28 MW biomass powerplant is developed in conjunction with concentrated solar power (CSP) Fresnel technology under the lenses of an exergetic analysis. This study broadens the comprehension about the diverse hybrid solar biomass configurations compared to the first law of thermodynamics analysis, resulting in new discussions and guidelines. Three configurations of CSP integrated into the powerplant is analyzed considering the northeastern semiarid region of Brazil for implementation. The yearlong simulation resulted in biomass economy from 1.9% to 9.7% and exergetic efficiency drop of 1.6% in the configuration with the higher solar contribution. The higher the solar input, the higher is the system exergetic efficiency drop. While the first law analysis suggests the lower temperature solar field to be the most efficient and the one to be invested, the second law analysis based on exergy suggest the opposite, recommending the higher temperature fields due to its lower exergy destruction.*

Keywords: *Hybrid powerplant. Solar energy. Biomass. Linear Fresnel. Exergy*

1. INTRODUCTION

With the Kyoto Protocol implemented in 2005, the participant countries had to seek new energy sources aiming to reduce their greenhouse gases (GHG) emission. Despite being a Kyoto Protocol member Brazil has built many non-renewable fired thermoelectric powerplants, increasing the concern with socio-environmental responsibility that affects the entire world. Although having a good share of renewable in its electricity generation mostly due the hydroelectric powerplants, Brazil must invest in newer technologies in renewable energy such as solar and wind to diversify its energy supply chain, decreasing its investments on the currently growing fossil fuel fired powerplants. Some developed countries, e.g. Denmark, aim to bring the amount of fossil GHG emissions to zero by 2050, doubling its use of biomass in thermoelectric powerplants (Barbosa, 2009).

Biomass fuels are a renewable energy source due to the relatively short crops life cycle. It represents 8.5% of the Brazilian energy mix, five times less than hydroelectric, but with positive growing rate. The Figure 1 shows the solar energy potential in South America and Western Europe for comparison, considering the annual averaged Direct Solar Irradiation (DNI) in kWh/m²y. Considering the 2019 Brazilian National Energy Balance (Balanço Energético Nacional, 2019) the internal supply of solar energy had a growth of 316.1%, despite the low contribution. In 2017 the Brazilian solar energy share corresponded to only 0.1% (832 GWh) and in 2018 it increased to 0.5% (3,461 GWh). Some comparison is possible to give a perspective of the untouched Brazilian potential on solar energy. The figure %% shows the DNI annual average for South America and Europe, in which is possible to verify that Germany has a much lower potential of solar availability than Brazil. The European country sunniest region has a similar annual DNI of the lower potential of Brazil. However, the German installed capacity of photovoltaic energy was 5.1 TWh in 2017 and 5.9 TWh in 2018. This country is experiencing a transition in the energy sector, reducing CO_2 levels by approximately 40% (IEEFA, 2020). Although the overall context for both countries are vastly different, the comparison over solar energy shows that Brazil has a great solar energy potential to be exploited and developed.

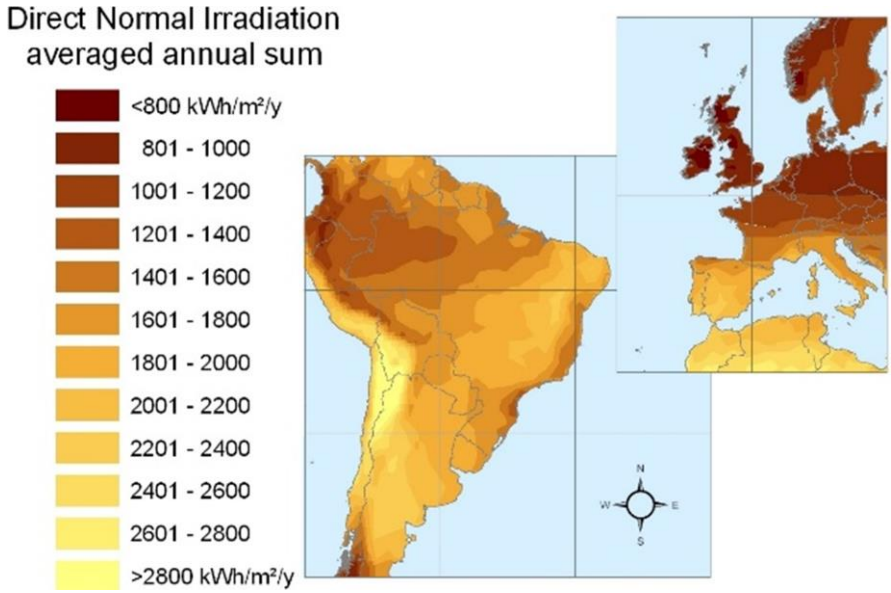

Figure 1. Averaged annual DNI for South America and Western Europe. Source: SolarPACES, 2020a

A hybrid solar/biomass energy configuration could work as a transition scenario to the Brazilian industries, supporting the investments with an already well-developed configuration such as biomass fired powerplants while developing the local technology for solar energy. In this scenario, the solar energy potential could be explored using the Concentrated Solar Power (CSP) technology.

The Table 1 shows the distribution of CSP projects in operation, under construction and under development in the world. Spain, for example, has 24.86% of the CSP projects in the world in operation.

Table 1. CSP projects in the world Source: SolarPACES, 2020b

Country	MW	%		Country	MW	%
USA	1740	18.78%		India	200	2.16%
Mexico	14	0.15%		Chile	1210	13.06%
Canada	1	0.01%		Australia	152.5	1.65%
Spain	2304	24.86%		Thailand	5	0.05%
Morocco	530	5.72%		South Africa	700	7.55%
Mena	1280	13.81%		Other	96	1.04%
China	1034	11.16%				
Total: 9266.5 MW						

The hybrid solar-biomass configuration is associated with better return of investment compared to the solar only powerplant, because it can supply uninterrupted energy with no need for energy storage, and also because it could have the advantage of an already installed transmission infrastructure. Considering the development required in the solar industry in Brazil, the Fresnel CSP technology is a well-suited entry option due to its simplicity in production. The Fresnel CSP technology concentrates the solar energy in tubes that are positioned in the focal line of the flat or slightly curved mirrors structure. The working fluid that passes through the tubes is heated by the solar energy, suppling heat to a Rankine cycle (Pitz-Paal, 2014).

Burin (2015), conducted a study for the hybridization of thermoelectric powerplants, using sugarcane bagasse as fuel, aiming to analyze the technical and economic feasibility of integrating parabolic concentrators. In that work, it was possible to improve the annual electricity production of these powerplants, maximizing their capacity factor. The biomass completed the natural solar energy intermittent behavior, resulting in a more reliable energy supply.

It is imperative to analyze the different hybrid configuration aiming its feasibility and performance. In this context the exergy analysis gives important parameters to evaluate the process, expanding the discussion from the first law of thermodynamics analysis. The exergetic analysis quantify the system irreversibility as the entropy is destroyed along the processes. As described by Shapiro (2009), the exergy quantifies the theoretical useful work to be extracted from a system, component, or energy stream. The exergetic analysis allows to identify the causes of irreversibility in a system, making it possible to compare different process configurations, select optimal process conditions and to decrease associated environmental impacts (Silva et al, 2018).

This work objective is to perform an exergetic analysis of a hybrid solar biomass powerplant, and to evaluate its best configuration as an option to diversify the Brazilian energy matrix.

2. METHODOLOGY

The thermoelectric powerplant which model is studied here is currently in operation and will be studied considering the city of Guanambi (14°12'S 42°46'W), located in the state of Bahia, Brazil. The powerplant has a limit capacity of 28 MW of electricity and can supply heat in a cogeneration cycle. Its boiler mass flow rate is equal to 100 ton/h. This region has a well-established forestry industry, and its biomass residues are suited to be used to operate the thermoelectric powerplant (ORLANDINI et al., 2011).

An efficiency comparison will be made for the solar hybridization in this powerplant for three solar fields configurations, modeled in accordance with the Linear Fresnel technology (Nova-1). A first law of thermodynamic analysis of this hybrid cogeneration powerplant was the focus of Galante (2015) work, whose representation is shown in Figure 2, followed by the system parameters described in Table 2. In this table is possible to verify the thermal efficiency for the Fresnel solar concentrator, $\eta_{Fresnel}$, in converting the solar thermal energy in thermal energy in the working fluid, a much lower value compared to the 85% boiler thermal efficiency. And in addition, the table shows the results obtained by the author for the solar to electricity efficiency, η_{SE}, which measures how much of the power generated in the system comes from the total solar power input.

The Rankine cycle, biomass combustion and boiler are modeled as described in the literature (Shapiro et al., 2009, Çengel, 2013 and Incropera et al., 2007). Then, the solar fields are combined considering the hourly solar collector efficiency and DNI data. Lastly, the exergetic analysis model for the hybrid powerplant is implemented to analyze which configuration results in the best application of the solar energy and infrastructure.

Solar field A will be designed to preheat the boiler feed water up to 185ºC when operating at its full design capacity. The Solar Field B is located parallel to the boiler and generates steam under the same pressure and temperature conditions required by the turbine. This second solar field was designed to provide up to 50% of the total boiler capacity. The solar field C must operate to generate dry saturated steam at 6495 kPa (280.8ºC) to be inserted directly into the boiler evaporator upper drum, with a maximum operating limit up to 50% of the boiler operating capacity.

The boiler model is required since each solar field modify its operating condition, leading it to a partial load fluctuating with different DNI for each hour of the day. It was used the log mean temperature difference (LMTD) method to implement this model, as described in Eq. (1) and Eq. (2). The Figure 2b shows a boiler representation with its air preheaters and economizer. All models were implemented using the Engineering Equation Solver (EES) software.

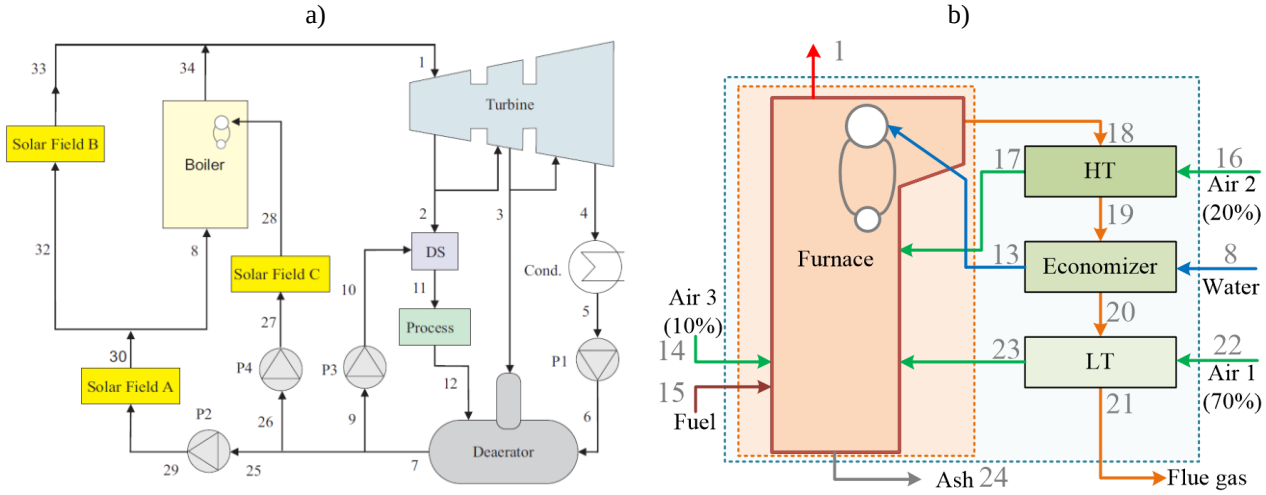

Figure 2 - a) Hybrid solar/biomass system. b) Representation of the boiler with exchanges. Source: Galante (2015).

Table 2 - Baseline system parameters for the biomass thermal powerplant. Source: Galante (2015)

Point	Temperature [ºC]	Mass flow rate [kg/s]	Pressure [kPa]	Quality
1	485	27.9	6495	-
2	-	-	900	-
3	-	-	250	-
4	51	-	Saturation	-
5	51	-	Saturation	0
6	-	-	250	-
7	110	-	250	-
8	-	27.9	6495	-
9	110	-	250	-
10	-	-	900	-
11	Saturation	≤ 6.94	900	1
12	Saturation	≤ 6.94	900	0

Parameters	Value
η_{boiler}	85%
η_{turb}	85%
η_{pump}	85%
DNI	0.433
η_{opt}	65%
T_{amb}	20ºC

$^{(1)}\eta_{Rankine}$	25.8%
$\eta_{Fresnel}$	39.9%
$\eta_{SE,A}$	14.2%
$\eta_{SE,B}$	12.9%
$\eta_{SE,C}$	13.8%

(1) considering the cogeneration process at full capacity.

$$\dot{Q} = UA \cdot MLTD \tag{1}$$

$$\dot{Q} = \dot{m}_{in} \cdot h_{in} = \dot{m}_{out} \cdot h_{out} \tag{2}$$

The solar fields model requires a yearlong computation for the Sun hourly position since the Fresnel CSP optical efficiency depends on the Sun incidence angles. The required angles were calculated according to studies developed by Spencer (1971). The Figure 3 a) shows the angles in relation to the horizontal plane *H* the plane in which the collector is located, as shown in Figure 3 b). With Eq. (3) and (4) it is possible to determine the solar declination angle, δ, that represents how far the Sun rises from the equator plane.

In addition to the solar declination, it is also required to calculate the solar incidence angle represented by θ, which is measured between the line that connects the Sun to the center of the Earth and the normal vector $\hat{n}$. In Eq. (5), the angle of solar incidence can be determined from the following parameters: the azimuth angle (γ), the latitude (ϕ) and the inclination angle β.

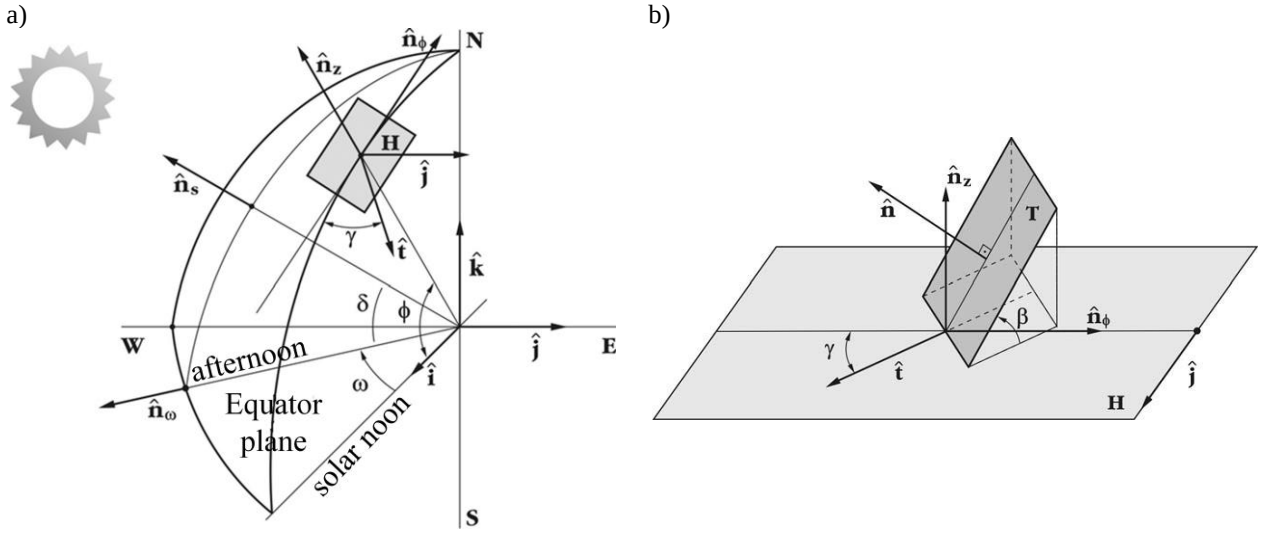

Figure 3. a) The Sun and horizontal plane H position in the celestial hemisphere. b) Solar field plane T in the H horizontal plane. Source: Galante, 2015

$$\delta = \frac{180}{\pi}\left(\begin{matrix}0.006918 - 0.399912\,cos(\Gamma) + 0.070257 sen(\Gamma) - 0.006758 cos(2\Gamma) \\ +0.000907 sen(2\Gamma) - 0.002697 cos(3\Gamma) + 0.001480 sen(3\Gamma)\end{matrix}\right) \tag{3}$$

$$\Gamma = \frac{360}{365} \cdot (n-1) \tag{4}$$

$$\cos(\theta) = \begin{pmatrix} sen(\delta)(sen(\phi)\cos(\beta) - \cos(\phi)\,sen(\beta)\cos(\gamma)) \\ +\cos(\delta)\cos(\omega)\,(\cos(\phi)\cos(\beta) + sen(\phi)sen(\beta)\cos(\gamma)) \\ +cos\,(\delta)sen(\beta)sen(\gamma)sen(\omega) \end{pmatrix} \quad (5)$$

Eq. (1) was used to find the thermal energy supplied by Novatec solar concentrators. This thermal energy depends on the area of solar field, the Direct Normal Irradiation (DNI), the optical efficiency factor (η_{opt}), and the receiver heat loss. The heat loss per square meter of solar field is calculated as shown in Eq. (6), also supplied by the manufacturer. In the yearlong solar field simulations performed in this work only DNI values higher than 0.05 kW/m² were considered.

$$Q_{solar} = A(DNI.\eta_{opt} - Q_{loss}) \quad (6)$$

$$Q_{loss} = 0.056 \cdot \Delta T_{sol}^2 + 0{,}000213 \cdot \Delta T_{sol}^2 \quad (7)$$

where

$$\Delta T_{sol} = \frac{T_{in} + T_{out}}{2} - T_{amb} \quad (8)$$

For the optical efficiency calculation in Nova-1 collectors it is necessary to use Eq. (9) which depends on the correction factors $K_I(\Theta_\perp)$ and $K_\parallel(\Theta_i)$, which are function of solar incidence angle, also provided by the Novatec (2020). The Table 3 shows K_I e K_{II} values versus the incidence angles.

$$\eta_{opt} = 0.67 \cdot K_I(\Theta_\perp)K_\parallel(\Theta_i) \quad (9)$$

Table 3 – Coeficients K_I and K_{II} as a function of angle θ. Source: Novatec Solar, 2020

θ	0º	10º	20º	30º	40º	50º	60º	70º	80º	90º
K_I	1	0.98	0.95	0.95	0.91	0.86	0.7	0.48	0.24	0
K_{II}	1	0.98	0.92	0.83	0.7	0.53	0.33	0.12	0.01	0

The energetic analysis follows as proposed by Bejan et al (1996). The Eq. (10) represents a specific exergy (kJ/kg), where e_{PH} represents physical exergy and e_{CH} chemical exergy.

$$e = e_{PH} + e_{CH} \quad (10)$$

Physical exergy is the maximum theoretical useful work obtained when the system goes from its initial state to the ambient condition, or dead state. Eq. (11) represents the specific physical exergy, associated with a mass flow (kJ/kg). This methodology requires to analyze each equipment in terms of its fuel and products, as shown in Figure 4.

$$e_{PH} = (h - h_0) - T_0(s - s_0) \quad (11)$$

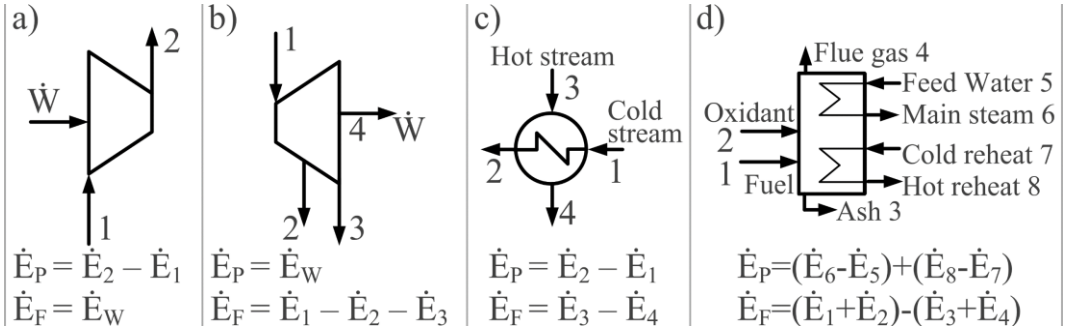

Figure 4 - Exergy rates of fuel and product for a) pump, b) turbine, c) heat exchanger, and d) boiler. Source: Bejan et al, 1995

The Eq. (12) proposed by Song et. al (2011) is used to calculate the chemical exergy of biomass.

$$e_{bio}^{ch} = 1812.5 + 295.606C + 587.354H + 17.506O + 17.735N + 95615S - 31.8A \quad (12)$$

where C, H, O, N and S are the percentages of carbon, hydrogen, oxygen, nitrogen, and sulfur in the chemical composition of biomass in wt%. The biomass considered in this work has the composition described in Table 4 in a dry basis, and it is considered that the biomass enters the furnace with a 50% moisture, *U*.

Table 4 - Percentage by weight of the chemical composition of biomass in dry basis, and the amount of moisture, *U*.

C	H	N	O	S	A	U
24,75	3,045	0,05	22	0,06	0,05	50.00

The components and system exergetic efficiency are defined by Eq. (13) e Eq. (14), respectively, considering that $\dot{E}_{F,sys}$ is the sum of fuel exergy rate that enters the overall system, in this case, the exergy rate of the biomass and exergy rate of the solar energy.

$$\varepsilon_E = \frac{\dot{E}_P}{\dot{E}_F} \quad (13)$$

$$\varepsilon_{E,sys} = \frac{\dot{E}_{p,sys}}{\dot{E}_{F,sys}} \quad (14)$$

The exergy destruction ratio y_D, Eq. (15), compares the exergy destruction rate of each component with the system fuel exergy rate. That is, $y_D$will be used to compare the performance between several components of the same system.

$$y_D = \frac{\dot{E}_D}{\dot{E}_{F,sys}} \quad (15)$$

3. RESULTS

The Table 6 shows the area required to meet each solar field design requirement. Although the solar field A receives the whole system water mass flow rate, it only needs to preheat the feed water up to 185ºC, resulting in the lower area required. The greater area is designed to solar field B, since it must warm, evaporate and superheat 50% of the whole system mass flow rate to the same conditions required by the turbine. The solar energy hybridization resulted in a fuel economy to the system. The yearlong simulation for the city of Guanambi lead to a reduction of 1.9% of fuel consumption with the solar field A operation, 9.7% fuel reduction to the solar field B, 6.2% reduction for a solar field B with 50% its projected area, and 7.8% fuel reduction for the solar field C. The solar field B 50% area reduction is aimed to analyze this parameter sensibility on fuel economy. A reduction of 50% of solar field area lead to a variation of only 36% in fuel economy. With a lower area, the solar field can operate more hours without reaching the thermal load limit $\dot{Q}max$, using more of the available solar energy.

Table 5. Solar field maximum design parameters and annual fuel economy.

Solar Field	T_{in} [°C]	T_{out} [°C]	Equivalent boiler flow rate	Area [m²]	$\dot{Q}max$ [kW]	Fuel economy
A	110.7	185	Always 100%	32,847	8,897	-1.9%
B	110.7	485	Up to 50%	162,807	40,612	-9.7%
B 50%	110.7	485	Up to 50%	81,403	40,612	-6.2%
C	110.7	280.8	Up to 50%	121,541	32,212	-7.8%

With the model based on the First law of thermodynamics it is possible to solve the properties for all the points in the system. The Table 6 shows the values for temperature, enthalpy, entropy and mass flow rate for the baseline model, with no solar energy, as illustrated in Figure 2a. The Figure 5 shows the boiler temperature distribution in two conditions: a) for the baseline, and b) for the feed water preheated to 185ºC by the Solar field A. This particular increased feed water temperature of 185ºC leads to a reduction in fuel consumption of 8.5% and thus a modified temperature and mass flow rate profile in this component. The boiler increased exergetic efficiency is a result of the lower exergy destruction rate inside this component since some of its preheating process now happens outside the boiler. However, it does not lead to a better exergetic efficiency for the overall system, since its exergy destruction rate is transferred to the Solar field A.

Table 6. Temperature, enthalpy, entropy, and mass flow rate for the system as shown in Figure 2a with no solar energy.

Point	Temperature [°C]	Enthalpy [kJ/kg]	Entropy [kJ/kg.K]	Mass [kg/s]		Point	Temperature [°C]	Enthalpy [kJ/kg]	Entropy [kJ/kg.K]	Mass [kg/s]
1	485.0	3380	6.79	27.9		12	175.4	742.9	2.09	6.9
2	243.4	2931	6.95	6.5		13	201.0	935.1	2.49	27.9
3	127.0	2714	7.46	1.5		25	111.0	461.4	1.41	27.9
4	47.5	2297	7.27	20.0		26	111.0	461.4	1.41	0.0
5	47.5	186.5	0.63	20.0		27	111.0	469.1	1.42	0.0
6	47.5	186.5	0.63	20.0		28	281.0	2778	5.85	0.0
7	110.0	461.4	1.41	28.3		29	111.0	469.1	1.42	27.9
8	111.0	469.1	1.42	27.9		30	110.7	469.1	1.42	27.9
9	110.0	461.4	1.41	0.4		32	110.7	469.1	1.42	0.0
10	110.1	462.2	1.41	0.4		33	485.0	3380	6.79	0.0
11	175.4	2774	6.62	6.9		34	485.0	2280	6.79	27.9

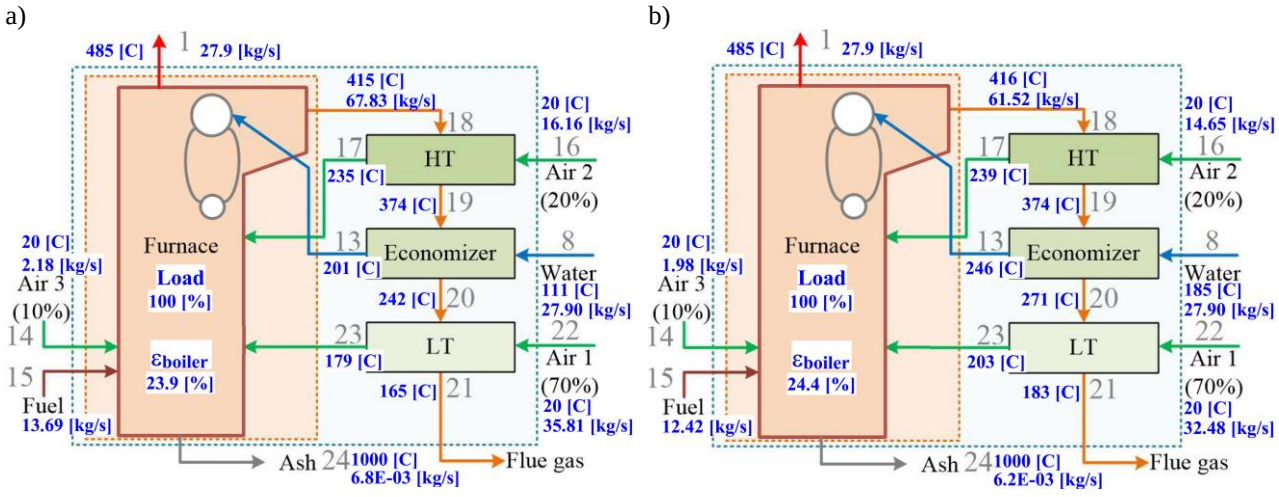

Figure 5. Boiler temperature profile for a) the baseline model, and for b) the boiler with increased feed water temperature by the solar field B.

The Figure 6 depicts the boiler thermal load behavior interacting with each solar field. For this specific day, the maximum DNI was higher than the one used to project the solar field areas. So, the amount of heat for each solar field was limited to its design condition to prevent operating the boiler beyond the desired limits. The flat lines for boiler and solar field thermal loads shows this operational limit in Figure 6 a), b) and c), for solar fields A,B and C, respectively. The Figure 6d shows a typical DNI curve for a high solar incidence day, with a peak around noon. Since the solar fields are limited to not absorb all the solar energy available, its exergetic efficiency drops, as they are not allowed to generated all their "products" with the "fuel" available, as described in Figure 4c.

The exergetic efficiency curves in Figure 6d goes in the opposite direction of the solar to electricity efficiency shown in Table 2, in which the solar field A has the better efficiency. Since the solar field A operates absorbing the high exergy content of solar energy and generates the product of lower temperature of all the fields, it is expected to have the lower exergetic efficiency among them. This is an indication that the high exergy solar energy is better used in higher temperatures designs delivering high exergy products. This is also a major contribution in understanding and project guidance over a single First law of thermodynamics analysis.

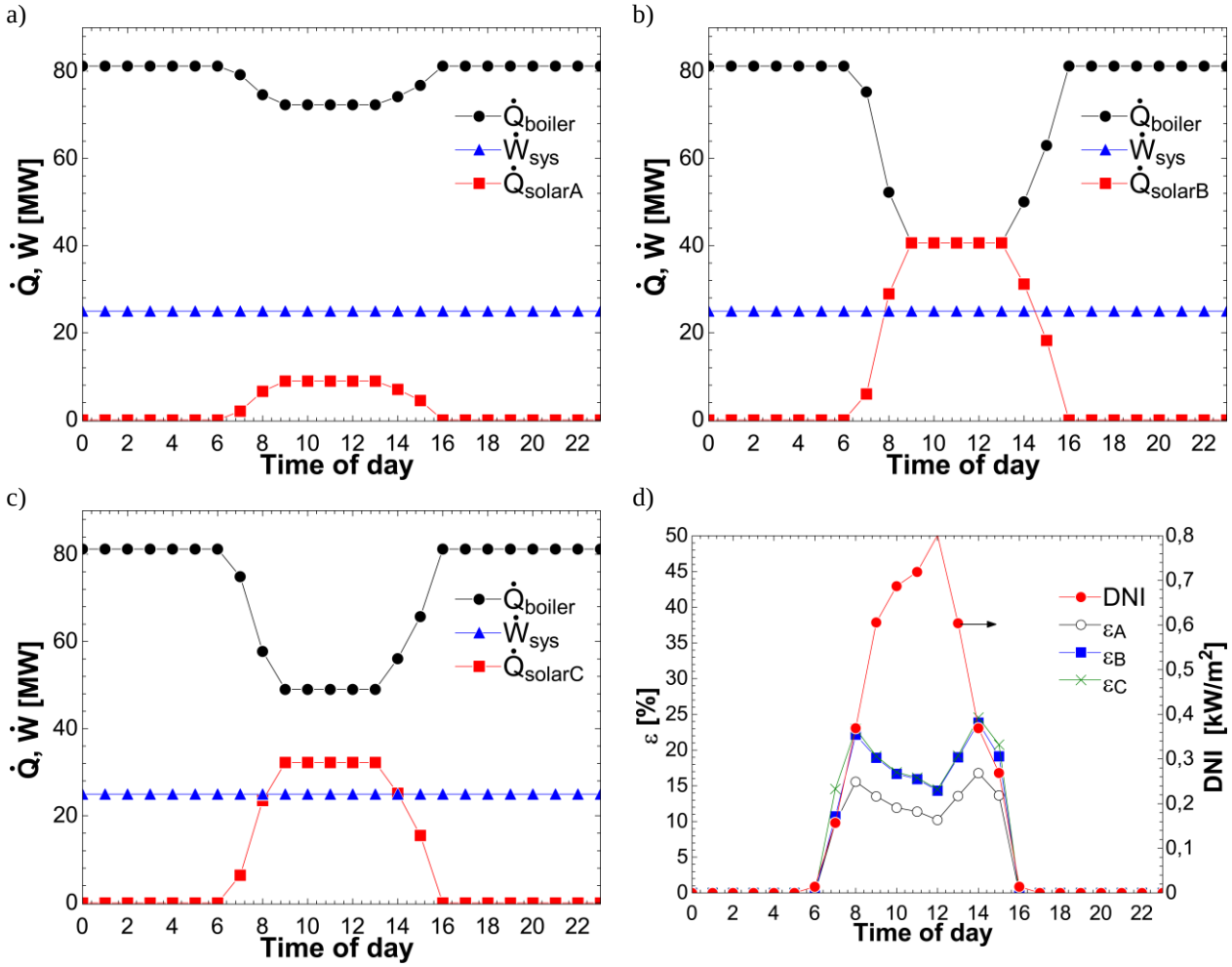

Figure 6 – Boiler and solar field thermal output and system power output for a) solar field A, b) solar field B, and C) solar field C. The item d) shows the exergetic efficiency for solar field as well the DNI for one day.

The Table 7 shows the exergetic efficiencies and exergy destruction ratio of the boiler and, furnace for each solar field implementation taking into account the values for the yearlong simulation. Comparing the furnace and boiler with no solar energy and with solar field A it is possible to verify only a slightly improvement in exergetic efficiency, mostly due to theirs lower exergy destruction while receiving feedwater in a higher temperature. The overall system only had a little reduction in performance with the solar field A since the feed preheating process now partially happens in an equipment with lower thermal efficiency. The same boiler, furnace and system behavior tendency is shown with solar fields B and C, only in different intensity depending on the solar energy contribution.

A major difference in results is seen when comparing the Solar B with Solar B DNI > 50 W. This later condition only shows the results for the hours in which the DNI was equal or higher than 50 W/m², eliminating from analysis the cloudy and night hours. It shows the values for boiler and furnace operating in partial load only, and therefore, with a lower rate of exergy destruction associate with the biomass combustion. Although the boiler and furnaces had a better exergetic efficiency, the system shows the effects of using the solar concentrators of lower thermal efficiency in order to generate the same power output in the turbine.

The scenario Solar B 50% has the same project conditions of Solar B, but half of its area. It leads to a lower solar contribution compared to the 100% area, and consequently, a higher boiler thermal load contribution and higher rate of exergy destruction. The exergetic efficiency, ε_E, is also higher since this value accumulates the night hours in which the boiler operates by its own with a higher thermal efficiency.

Table 7. Annual averaged exergetic efficiency and energy destruction ratio for the baseline system, with operating solar fields A, B and C, and solar field B with no dark hours (DNI > 50 W) and with 50% of original area.

Components	No solar		Solar A		Solar B		Solar B DNI > 50 W		Solar B 50%		Solar C	
	ε_E [%]	y_D [%]	ε_E [%]	y_D [%]	ε_E [%]	y_D [%]	ε_E [%]	y_D [%]	ε_E [%]	y_D [%]	ε_E [%]	y_D [%]
Boiler	25.8	69.2	26.0	67.3	25.8	60.5	25.9	43.4	25.8	64.7	28.3	62.6
Furnace	24.8	66.5	24.9	64.7	24.8	58.2	24.9	41.9	24.8	62.2	24.9	60.1
System	27.6	72.4	27.3	72.7	26.0	74.0	23.1	76.9	27.0	73.0	26.5	73.5

The Figure 7 illustrates the effect of lowered system exergetic efficiency with the participation of solar energy for each solar field in comparison with the baseline system with no solar energy, ε_{sys}. Although the solar field A is the solar field with lower exergetic efficiency, this is also the one with lower impact in the system due to its lower solar energy contribution. The solar field B, the one with the higher contribution of solar energy, is also the one that causes the higher impacts on exergetic efficiency.

It is inherent to the hybrid solar biomass power system that a certain amount of solar energy is rejected. An exception to this would happen for an undersized solar field, in which the boiler lower capacity would not be reached. On the other hand, an oversized solar field would reject too much solar energy, decreasing the system exergetic efficiency. Since the solar hybridization leads to a reduction of exergoeconomic efficiency, the higher ε_E happens with no solar energy at all. Therefore, an optimization of the solar field area would require a thermoeconomic analysis, such as the exergoeconomic analysis, in which the optimization would seek a financial balance for the system based on the flow of exergy and costs. Considering the financial aspects, the solar energy may contribute to lower the costs with fuel, while being backed up by the biomass in the cloudy and night hours, resulting in a steady energy supply.

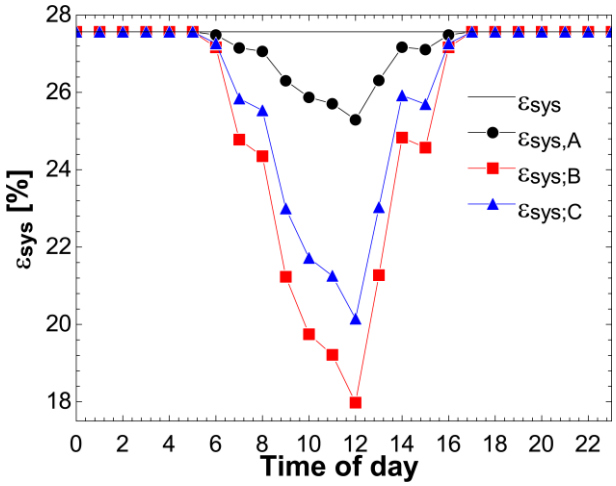

Figure 7. System exergeconomic efficiency for the baseline and for each hybrid solar field configuration.

4. CONCLUSIONS

A model for a hybrid solar biomass power plant was developed in this work based on the first and second laws of thermodynamics. The Rankine cycle and boiler were modeled taking an existing biomass powerplant currently in operation, and its integration with solar energy was examined for three configurations. The model allows a yearlong simulation of solar incidence and solar energy conversion to thermal energy considering the concentrated solar power (SCP) Fresnel technology.

The hybrid solar biomass configuration was designed considering the baseline biomass operational requirements in a way that would supply a steady power output even with the intrinsic solar intermittency, eliminating the need of expensive and complex thermal storage.

The exergetic analysis expands the understand of efficiency for the solar fields aiming power generation. While the first law analysis suggests the solar field A with the higher efficiency, the exergetic analysis results in the solar field A with the lower field efficiency due to its lower temperature products. Since the solar fields have a lower efficiency in converting thermal energy to the working fluid when compared to the boiler, any solar contribution will lead in reduction of the system exergetic efficiency. It suggests that an optimal configuration for solar field is possible to be found in a thermoeconomic analysis, such as the exergoeconomic analysis. This work gives an extra step forward the hybrid solar biomass power plant and recommends an exergoeconomic analysis for future works.

5. ACKNOWLEDGEMENTS

To the Federal Technological University of Paraná, UTFPR Campus Guarapuava, for support during research.

6. REFERENCES

BARBOSA, D. “Dinamarca aposta na energia dos ventos para ter eletricidade de baixo carbono”. Avaiable at: <http://g1.globo.com/noticias/ciencia/0,,mul1410982-5603,00-dinamarca+aposta+na+energia+dos+ventos+para+ter+eletricidade+de+baixo+carbo.html>. Accessed: 15 out. 2020.

BEJAN, A. et al. *Thermal Design and Optimization*. John Wiley & Sons, 1996.

Balanço Energético Nacional 2019. Avaiable at: <https://www.epe.gov.br/pt/publicacoes-dados-abertos/publicacoes/balanco-energetico-nacional-2019>. Accessed: 15 out. 2020.

BURIN, Eduardo Lucas Konrad. *Plantas de cogeração do setor sucroalcooleiro assistidas por concentradores parabólicos*. 2015. 157 p. Tese (Doutorado) - Universidade Federal de Santa Catarina, Centro Tecnológico, Programa de Pós-Graduação em Engenharia Mecânica, Florianópolis, 2015.

ÇENGEL, Yunus A.; BOLES, Michael A. *Termodinâmica*. 7. ed. Porto Alegre: AMGH, 2013. xxviii, 1018 p. ISBN 9788580552003.

GALANTE, Renan Manozzo. *Análise termodinâmica de uma planta termoelétrica a biomassa assistida por energia solar*. 2015. 120 p. Dissertação (Mestrado) - Universidade Federal de Santa Catarina, Centro Tecnológico, Programa de Pós-Graduação em Engenharia Mecânica, Florianópolis, 2015.

IEEFA. “Germany sets new record for solar generation. Institute for Energy Economics & Financial Analysis”, 21 abr. 2020. Avaiable at: <https://ieefa.org/germany-sets-new-record-for-solar-generation/>. Accessed: 15 out. 2020

Incropera, F.P.; Dewitt, D.P; bergman, T.L.; Lavine, A.S., 2007. *Fundamentals of heat and mass trasnfer*. John wiley & sons, inc.

Novatec solar. 2020. “Nova 1”. <http://novatecsolar.com/files/mn1102_nova1_brochure_eng_web.pdf> (accessed 10.07.2020).

ORLANDINI, D. et al. Potencialidades das regiões brasileiras para instalação de uma fábrica de celulose. *Revista Árvore*, v. 35, n. 5, p. 1053–1060, out. 2011.

Pitz-Paal, R., 2014. Chapter 19 Solar Energy - Concentrating Solar Power. In: LETCHER, T. M. (Ed.). *Future Energy*. Oxford: Elsevier. p. 405-431.

Shapiro, H.N.; Moran, M.J., 2009. *Princípios de termodinâmica para engenharia*. 7ª ed. Rio de janeiro: ltc (grupo gen), 864p.

Silva, S. R., Niquini, G. R., Turetta, L. F., Costa, A. O. S., 2018. Aplicação da Propriedade Termodinâmica Exergia na Avaliação de Processos de Produção de Etanol Lignocelulósico: Uma Revisão. *Revista virtual de Química. Universidade Federal de Mina Gerais*, Belo Horizonte, Brasil.

SolarPACES 2020a. “Potential for Solar Thermal Energy By Country”, Avaiable at: <https://www.solarpaces.org/csp-technologies/csp-potential-solar-thermal-energy-by-member-nation/>. Accessed: 15 out. 2020

Solarpaces 2020b. “CSP Projects Around the World” Avaiable at: < https://www.solarpaces.org/csp-technologies/csp-projects-around-the-world/>. Accessed: 10 jun. 2020

Song, G.; Shen, L.; Xiao, J., 2011. Estimating specific chemical exergy of biomass from basic analysis data. *Industrial & engineering chemistry research*, v. 50, n. 16, p. 9758–9766.

Spencer, J. W. *Fourier series representation of the position of the sun*. 1971.

7. RESPONSIBILITY NOTICE

The authors are the only responsible for the printed material included in this paper.